https://doi.org/10.1016/j.engstruct.2020.111618

Cold-Formed High Strength Steel Tubular Beam-Columns

Jia-Lin Ma[a], Tak-Ming Chan[b*], Ben Young,[b]

[a]Building Research Center, Vanke Co. Ltd., Huanmei Rd., Shenzhen 518000, China.
[b]Dept. of Civil and Environmental Engineering, The Hong Kong Polytechnic University, Hong Kong, China

Abstract:

High strength steel is used more often in a variety of civil engineering applications due to its high strength-to-weight ratio and cost effectiveness. This paper presents the experimental investigation on cold-formed high strength carbon steel tubular members subjected to combined compression and bending. The nominal 0.2% proof stresses of the test specimens were 700 and 900 MPa. The test specimens consisted of square hollow sections (SHS), rectangular hollow sections (RHS) and circular hollow sections (CHS). The material properties, global geometric imperfections of the specimens were measured. The behaviour of the beam-column members was investigated through testing 32 specimens which had a nominal member length of 1480 mm. The second order effects were also considered by measuring the mid-height deflections for all specimens. The compression and bending capacities, load-deformation histories and failure modes of the test specimens were also reported. The test results were compared with the values predicted from the American, Australian and European standards. Improved design recommendation is provided for cold-formed high strength steel tubular beam-columns. Based on the experimental results, finite element modelling methodology is also proposed.

Keywords: Cold-formed steel; Global geometric imperfection; High strength steel; Beam-column; Combined loading test; Tubular section.

1 Introduction

High strength steel (HSS) structural sections have higher strength-to-weight ratios and lower material costs when compared with mild steel sections. HSS tubes with nominal yield strengths of 700 and 900 MPa as well as other steel grades are now available in the market. The potential use of HSS can help achieving more economic design in steel structures.

Studies have been conducted to investigate the compression behaviour of fabricated HSS members in the past decades [1-3]. The bending behaviour of fabricated HSS members have also been studied [4-7]. Investigations on the compression behaviour and bending behaviour of cold-formed HSS circular hollow section (CHS) members were conducted by Zhao [8] and Jiao and Zhao [9]. Recent studies on the column and beam behavior of cold-formed HSS ($\sigma_{0.2} \geq 700$MPa) square hollow sections (SHS), rectangular hollow sections (RHS) and circular hollow sections (CHS) have been carried out by the authors Ma et al. [10-12]. Structural members subjected to combined compression and bending (beam-columns) are widely used in various constructions. Early investigation on high strength steel beam-columns have been conducted for fabricated I- and box-sections in Yu and Tall [13] and Usami and Fukumoto [14]. Conclusions given in previous literatures showed that, when compared on a non-dimensional basis, the strength of built-up high strength steel columns exceed those of ordinary steel columns. Recent research on press-braked S690 high strength steel angle and channel stub columns, S960 press-braked channel columns, fabricated S690 I-section beams and stub columns have also been conducted [15-18]. Research on cold-formed high strength ($\sigma_{0.2} \geq 700$MPa) carbon steel SHS, rectangular hollow sections RHS and circular hollow sections SHS beam-columns are rarely found in the literature. The authors investigated cold-formed high strength steel rectangular and square hollow sections under combined compression and bending in Ma et al. [19].

This paper presents the experimental investigation on HSS tubular sections under combined compression and bending. The beam-column specimens in this paper had 2 different grades: namely, H-series and V-series having the nominal proof stresses of 700 and 900 MPa, respectively. The tubes are in compliance with EN10219 hollow sections. The test results are compared with the predicted values calculated from American, Australian and European codes to examine their applicability for HSS tubular beam-columns.

2 Experimental Investigation

2.1 Test Specimens

Cold-formed high strength steel (HSS) members in three cross-sections (H80×80×4, H100×50×4 and V89×3) were tested under combined compression and bending in this study. The square hollow sections (SHS), rectangular hollow sections (RHS) are labelled as "Series, *B*, *H*, *t*" and the circular hollow sections (CHS) are labelled as "Series, *D*, *t*", in which *B*, *H*, *D* and *t* are the width, depth, outer diameter and thickness of the sections, respectively. The specimens were cold-formed and welded longitudinally using the high frequency welding technique.

High strength steel (HSS) gains strength through hot-rolling or cold-working process and it is different from mild steel as there is no yield plateau. The 0.2% proof stress $\sigma_{0.2}$ is usually taken as the yield stress f_y. To examine the material properties of those sections, standard tensile coupons were prepared and tested on a 50 kN capacity MTS machine. The tensile test coupon specimens were cut longitudinally along the tubes. Measured on a 25mm gauge length, the elongation of specimens ranged from 10% to 17%. The measured basic material properties are obtained from the static stress-strain curves and summarized in Table 1. The obtained full stress-strain curves are plotted in Fig. 1. A more comprehensive study on the material properties, strength variations and the residual stress distributions over the HSS sections has been reported in Ma et al. [12].

All the beam-column specimens were cut into length of 1480 mm and milled flat on both ends before being welded to end plates. The dimensions of the specimens are reported in Table 2 – 5. Axial compression and uniaxial bending were applied to the specimens. Thus for H100×50×4, the tests were conducted in two series for major axis bending as well as minor axis bending. The specimens were labelled as "Series, *B*, *H*, *t,* BC, eccentricity" for SHS/RHS and "Series, *D*, *t,* BC, eccentricity" for CHS so that the nominal cross-section geometry, loading eccentricities could be identified (e.g. H50×100×4-BC-e3 stands for a beam-column 'BC', which bends in its major axis and is loaded with a nominal eccentricity of 3 mm at both ends.). R and r are the outer and inner corner radii for the SHS and RHS. The cross-section area A, elastic (W_{el}) and plastic (W_{pl}) section moduli are also calculated and reported in the tables. Totally 32 beam-column specimens were tested in this study. The specimens were grouped into 4 series according to the sections. In each series, one specimen was loaded concentrically with the eccentricity smaller than 0.3 mm, whereas the other 7 beam-columns were loaded with different eccentricities. Among the 7 beam-columns in each series, one of the eccentricities was repeated and the repeated test was labelled with a '#' at the end of the specimen label. The measured eccentricity values ($e+\delta_0$) that include the global imperfections δ_0 are reported in the last column of the tables.

2.2 Global Geometric Imperfection Measurements

Steel tubes are usually inherited with geometric imperfections which can affect the structural performance. In this experimental investigation, global buckling was the dominant mode of failure and the effect of local geometric imperfections is thus insignificant. Hence, only initial global geometric imperfections of the beam-columns were measured and reported in this study. A Leica TCR405 total-station was used to obtain readings at mid-height and near both ends of the specimens. The geometric imperfections were measured at the flat width near the corner for SHS and RHS and at the extreme fiber on the right hand side for CHS. The sign convention and the location of measurement are shown in Fig. 2. The measured values are summarized in Table 6 and normalized to the specimen lengths. The average absolute value of the global geometric imperfections at mid-height were $L/3714$, $L/3479$, $L/4107$ and $L/7117$ for specimens in test series H80×80×4-BC, H100×50×4-BC, H50×100×4-BC and V89×3-BC respectively. These measured values are relatively small when compared to widely-used global geometric imperfection values of $L/1000$ and $L/1500$.

2.3 Four Point Bending Tests

To evaluate the performances of beam-column specimens, it is important to know the bending capacities of the sections in order to obtain the complete experimental interaction data. The pure bending moment capacities of the sections are obtained through four point bending tests and reported in Ma et al. [10]. Owing to the section shapes and test setups, lateral torsional buckling of beams was restricted. The cross-sectional bending moment capacities for the four series in this study are summarized in Table 7. Letter 'B' as shown in the suffix of the specimen label indicates the beam specimens.

2.4 Combined Compression and Bending Tests

Totally 32 long HSS beam-columns were tested in this study. The beam-column specimens were cold-sawed from 3 m long tubes. The cut tubes were then manufactured into 1480mm long specimens. They were milled flat on both ends before being welded onto 25 mm thick end plates. The test rig and setup are shown in Fig. 3. A hydraulic testing machine with 1000kN capacity was used to apply compressive force to the specimens. The specimens were compressed between two parallel knife edges, which were formed by sets of pit plates and wedge plates. The knife edges allow the specimen to rotate in the bending plane. Slot holes were machined on the wedge plates to allow adjustment of the loading eccentricities onto the specimens at both ends. The upper pit plate was fixed, whereas the lower pit plate was installed on a lockable special bearing. The specimen was first installed onto the wedge plates using bolts and then put between the pit plates in the test rig. The lower special bearing is free to rotate during preloading to eliminate any possible gaps between the specimen and the bearings. The special bearing was locked throughout the tests after the preloading.

Three displacement transducers were used to measure both the axial shortening and end-rotation of the specimens. In addition, two transducers were setup at the mid-height of the specimen on the two sides in the bending plane to capture the horizontal deflection of the beam-columns during loading. To determine the loading eccentricities, four strain gauges were attached on the two faces in the bending plane for SHS and RHS, as shown in Fig. 4. Similarly, for CHS, two strain gauges were applied at the extreme tensile and compression fibers at mid-height of the specimens. Displacement-control was used to apply the axial compression load to the specimens. A fixed loading rate of 0.5 mm/min was used for all the tests. The static responses of the beam-columns were captured through pausing the tests near ultimate for 90 seconds. Loads, readings from transducers and strain gauges were recorded at a regular interval by a data acquisition system.

2.5 Determination of the loading eccentricities

The loading eccentricities for beam-columns were carefully measured. Before testing, the specimen was installed on the wedge plates with a designated eccentricity and then pre-loaded with 3 kN to ensure everything were in full contact and the beam-column was in an up-straight position. The bottom special bearing was then locked by bolts after pre-loading. Four strain gauges and two horizontal transducers were connected to the data acquisition system to obtain the strain and deflection at mid-height of the beam-column.

The centers of the specimens were carefully marked at mid-height on the front face before tests. The applied eccentricity was first measured by the total station through comparing the space coordinates of the center point on the front face of the specimen and the front center of the knife edge, which is named the total station method hereafter. When the tests started, the bending moments of the specimens at mid-height is known to be equal to $EI\kappa$ during elastic response of the members, in which EI is the flexural rigidity of the cross-section in the bending plane, and κ is the curvature calculated from the strain gauge readings. Therefore, the loading eccentricity ($e+\delta_0$) can be calculated from $(e+\delta_0)=EI\kappa/P-\delta_y$, in which δ_0 is the initial global geometric imperfection and δ_y is the horizontal deflection calculated from the absolute average readings of the two horizontal transducers. This is hereafter called the strain gauge method. Similar approaches were used in Zhu and Young [16] and Huang and Young [17]. The strain gauge method was used for eccentricities up to 50 mm. For specimens with eccentricity greater than 50 mm, the total station method was used. The results for eccentricity measurements are summarized in the last columns of Table 2 to Table 5.

2.6 Test Results and Design Assessment

The axial load P versus the end moment M_{end} and mid-height moment M_{mid} curves for the beam-columns are shown in Fig. 5-8, in which the ultimate points are marked with red circles. The beam-columns all failed by flexural buckling, and most of them shown large second-order effects under axial loads. The experimental ultimate loads P_{exp}, end moment $M_{end,u} = P_{exp}e$, mid-height moment $M_{mid,u}=P_{exp}(e+\delta_0+\delta_y)$ and end rotation θ corresponding to ultimate axial loads are given in Table 8. The ultimate values are also compared with the code predictions from AS 4100 [18] (P_{AS}), ANSI/AISC 360-10 [19] (P_{AISC}) and EN 1993-1-1 [20] (P_{EC3}). Corresponding design interaction equations are given in Table 9.

According to previous investigation on cold-formed high strength steel tubular beams [10], the pure bending capacities were underestimated by the specifications for square and rectangular sections. AS 4100 [22] and ANSI/AISC 360-10 [23] gave conservative predictions for circular hollow section specimens under pure bending. Therefore, gaps between dots (moment capacities of the beam tests) and interaction end points were observed on the horizontal axis for the interaction curves. For concentric loadings, conservative predictions were observed for H50×100×4 which is compact when bending about the major axis.

In EN 1993-1-1 [24] different buckling curves were adopted to describe the flexural buckling behavior of steel members. The specimens were categorized to use buckling curve 'c' because of cold-forming. In this paper, improvements were later to EN 1993-1-1 [24] and the comparison to EN 1993-1-1 [24] using the buckling curve 'a' instead of curve 'c' is given in the last column of Table 8 as P_{exp}/P_{EC3}^{*}.

The comparisons were made to the points on the interaction curves which have the same initial loading eccentricities e as the tested specimens. Generally, these standards underestimate the loading capacities of HSS tubular beam-columns by 3 to 14% on average. For specimens with measured eccentricities smaller than 0.3 mm, they were treated as concentrically loaded columns and the axial loading capacities were compared to the column capacities calculated from the codes.

The experimental ultimate loads P_{exp}, end moment $M_{end,u}$ are normalized to the average section squash load $P_y=Af_y$ and plastic moment $M_p=W_{pl}f_y$ respectively, and are plotted against the normalized interaction curves from the codes in Fig. 9 to Fig. 12.

In EN 1993-1-1 [24], the specimens of CHS V89×3 were grouped into class 4. However, previous research for HSS stub columns and beams had proved that the slenderness limits were not applicable for HSS CHS, and predictions for CHS stub columns and beams from EN 1993-1-6 [25] were conservative by 17% and 47%, respectively [10-11]. Chan et al. [26] proposed a new yield slenderness parameter $D/[t(480/f_y)]$ instead of $D/[t(235/f_y)]$ for high strength steel CHS. The tested beam V89×3-B had the ultimate moment larger than the section plastic moment, hence they should be classified as class 2 or above. As a result, specimens in series V89×3-BC in this study were all calculated as class 2 for EN 1993-1-1 [24]. The interaction curves in the graphs were calculated based on method 1 in Annex A for the four series of specimens. Average geometries were used in evaluating the interaction curves for each test series. Eurocode apply different column buckling curves for various types of specimens. The cold-formed HSS columns are designated to use the buckling curve 'c' whereas clearly the axial compression capacity for HSS columns were underestimated by more than 20% for the concentrically loaded columns with eccentricity smaller than 0.3 mm. Thus, another set of evaluation (P_{exp}/P_{EC3}^*) was made which adopted the column buckling curve 'a' and the comparison is shown in the last column of Table 8. The interaction curves using column buckling curve 'a' were also plotted in Fig. 9 to Fig. 12 as dotted lines. The predictions were improved by 10%.

Interactions curves obtained from AS 4100 [22] and ANSI/AISC 360-10 [24] are also shown in Fig. 9 to Fig. 12. Both standards apply the end moment amplification factor $1/(1-P/P_{cr})$ to consider the second order effect for members with equal bending moments at the ends. Non-linear interaction curve can be obtained if end-moments are used for comparison. However, ANSI/AISC 360-10 [23] uses a two-phase relationship to describe the interaction of axial loads and bending moments for the beam-columns, and the predictions from ANSI/AISC 360-10 [23] are the closest. Generally, the capacities of HSS specimens against pure compression and pure bending are underestimated by the three standards, which leads to the conservative predictions for beam-column results (10%, 3% and 14% on average). Further research is needed to propose modifications on the existing standards to improve the predictions.

3 Finite Element Modelling

In this section, the finite element modelling methodology on cold-formed high strength steel (HSS) tubular beam-columns is presented. The obtained constitutive models from tests have been presented in Ma et al. [12]. The stress-strain relationship for Abaqus should be defined in the format of true stress versus log plastic strain, thus the measured engineering stress-strain curves were converted using the definition in the Abaqus manual. The S4R shell element with 4 nodes and reduced integration was used [27]. The mesh seed sizes (B+H)/30 and D/15 were adopted for RHS/SHS and CHS, respectively. Similar models have been successfully adopted to replicate the behavior of cold-formed HSS tubular stub columns and beams [10-11]. The lowest elastic eigenmode shape was chosen as the global geometric imperfection profile. The bow shape profiles (Fig. 13) obtained from the buckle analysis were scaled to the measured global imperfection values in Table 6 and later adopted for FE analysis.

The sections are compact enough thus no local buckling were observed throughout the tests. Trial models were built and results showed that the influence of local geometric imperfections to member ultimate loads was insignificant. In the longitudinal direction, large bending residual stresses and small membrane residual stresses were found from a residual stress study on three cold-formed HSS sections [12]. The nature of tensile coupon tests made it possible to include the large bending residual stresses in the tested constitutive relationships [28]. Meanwhile, the largest measured longitudinal membrane residual stresses of HSS tubes were reported to be only about 20% of the 0.2% proof stresses and their influence upon the finite element models was negligible [12]. Thus the inclusion of geometric local imperfections and residual stress in the models were not necessary.

The corner strength enhancements in SHS and RHS should be considered because of the large amount of cold-working during the process of cold-forming the high strength steel sections. The constitutive relationships for corner portions of different sections have been obtained from corner tensile coupon tests in Ma et al. [12]. Therefore, the cold-working effect was taken into consideration by assigning the extended corner regions in the FE model. Corner extension with length of $2t$ was suggested in [11, 29-30]. The finite element HSS beam-column models in this study thus adopted this methodology for SHS and RHS beam-column members, as shown in Fig. 14.

To simulate the boundary conditions of concentrically and eccentrically loaded beam-columns, two reference points at the location of top and bottom pins were set. At each end of the specimen, the endplate, wedge plate and the pin have a total height of 87.5 mm, thus the reference points were offset by 87.5 mm longitudinally and then coupled to the nodes of top and bottom cross-section ends, respectively, as shown in Fig. 15. Hence the effective lengths of the specimens were accurately modeled. On the two reference points, the rotation in the bending plane is allowed and the translation of the top reference point in the longitudinal direction is also possible. Compression forces were applied to the specimens through the top reference point in a Static, Riks analysis step. The geometric non-linearity was enabled throughout the analysis and the maximum step increase was limited in order to obtain smooth load-deformation histories.

The test-to-finite element ultimate capacity ratios for the model are tabulated in Table 10. Results showed that the model predict the test ultimate capacities of beam-columns closely within 3% on average. The comparisons of the load-deflection curves and failure modes are also given in Fig. 16-17 and Fig. 18. The general form of load-deflection response and failure modes were successfully captured. The good replication of ultimate capacities and failure modes proved the validity of above-mentioned assumptions and the effectiveness of the finite element modelling methodology.

4 Conclusions

This paper presents the experimental investigation on cold-formed high strength steel (HSS) with nominal yield strengths of 700 and 900 MPa tubular members subjected to combined compression and bending. Four series of tests (H100×50×4-BC, H50×100×4-BC, H80×80×4-BC and V89×3-BC) were conducted for different sections, in which the RHS 100×50×4 was tested for both major and minor axes bending. Design strengths calculated by ANSI/AISC 360-10 [23] matched well with the experimental results but the evaluation from AS 4100 [22], and EN 1993-1-1 [24] were conservative by around 10%. Illustrations were given to compare the normalized test results against normalized interaction curves predicted from the standards. The current standards recently extended the use of high strength steel with nominal yield stress less than 690 MPa, but the design rules have not yet been verified comprehensively for high strength steel members. The current specifications are found to be conservative, because the capacities of specimens are underestimated for either pure compression or pure bending. It is shown that ANSI/AISC 360-10 [23] give the best predictions for this batch of HSS beam-columns. For the European code EN 1993-1-1 [24], the slenderness limit for CHS should be modified and the column buckling curve ‘a’ is more suitable than curve ‘c’ for high strength steel members. Numerical investigation was also performed to validate the proposed finite element modelling methodology for cold-formed high strength tubular beam-columns. The experimental investigation provides a concrete base for future study regarding high strength steel tubular beam-columns.

5 Acknowledgements

The authors would like to thank the technicians and the final year undergraduate student Mr. Ho-Chun Chui from the Department of Civil Engineering at The University of Hong Kong for their assistance in helping the experimental works. The authors are also grateful to Rautaruukki for supplying the cold-formed high strength steel tubular test specimens. The research work described in the article was supported by a grant from the Research Grants Council of the Hong Kong Special Administrative Region, China (Project no. 17212115).

6 Notation

The following symbols are used in this paper:

A = Gross cross section area;

B = Overall width of cross section;

D = Outer diameter of circular hollow section;

E = Young's modulus of steel;

e = Loading eccentricity;

f_y = Yield stress of steel;

H = Overall depth of cross section;

I = Second moment of area;

k_{yy} = Interaction factor from EN 1993-1-1

L = Length of beam column;

M_{end} = Experimental moment at specimen ends;

$M_{end,u}$ = Experimental ultimate moment at specimen ends;

M_{mid} = Experimental moment at mid-height;

$M_{mid,u}$ = Experimental ultimate moment at mid-height;

M_p = Plastic moment of cross-section;

M_n = Nominal flexural strength of cross-section

M_u = Ultimate moment of cross-section

P = Axial load;

P_{AISC} = Nominal strength (unfactored design strength) from ANSI/AISC 360-10;

P_{cr} = Elastic critical buckling strength of the member;

P_{AS} = Nominal strength (unfactored design strength) from AS 4100;

P_{EC3} = Nominal strength (unfactored design strength) from EN 1993;

P_{EC3}^{*} = Nominal strength (unfactored design strength) from EN 1993 using buckling curve ‘a’;

P_{exp} = Experimental ultimate load;

P_n = Nominal compressive strength

P_y = Squash load of cross-section;

P_u = Ultimate strength of column

R = Outer corner radius of square and rectangular hollow sections;

r = Inner corner radius of square and rectangular hollow sections;

t = Plate or wall thickness;

W_{el} = Elastic section modulus;

W_{pl} = Plastic section modulus;

δ_0 = Measured global geometric imperfection;

δ = Horizontal deflection at mid-height of specimen;

κ = Curvature of specimen at mid-height;

σ_u = Static ultimate tensile strength;

$\sigma_{0.2}$ = Static 0.2% tensile proof stress;

ε_{25mm} = Non-proportional elongation at fracture based on 25 mm gauge length.

θ = End rotation of specimens

7 References

[1] Nishino, F., and Tall, L. "Experimental investigation of the strength of T-1 steel columns." *Fritz Engineering Laboratory Report*, Lehigh University, Bethlehem, Pennsylvania;1970.

[2] Nishino, F., Ueda, Y., and Tall, L. "Experimental investigation of the buckling of plates with residual stresses." *Fritz Engineering Laboratory Report*, Lehigh University, Bethlehem, Pennsylvania; 1966.

[3] Rasmussen, K. J. R., and Hancock, G. J."Plate slenderness limits for high strength steel sections." *Journal of Constructional Steel Research.* 1992; 23(1-3):73-96.

[4] Beg, D., and Hladnik, L. "Slenderness limit of class 3 I cross-sections made of high strength steel." *Journal of Constructional Steel Research*. 1996; 38(3): 201-217.

[5] Green, P. S., Sause, R., and Ricles, J. M. (2002). "Strength and ductility of HPS flexural members." *Journal of Constructional Steel Research.* 2002; 58(5-8): 907-941.

[6] Lee, C. H., Han, K. H., Uang, C. M., Kim, D. K., Park, C. H., and Kim, J. H. "Flexural strength and rotation capacity of I-shaped beams fabricated from 800 MPa steel." *Journal of Structural Engineering. 2012;* 139(6): 1043-1058.

[7] Ricles, J. M., Sause, R., and Green, P. S. "High-strength steel: implications of material and geometric characteristics on inelastic flexural behavior." *Engineering Structures*. 1998; 20(Nos 4-6): 323-335.

[8] Zhao, X. L. "Section capacity of very high strength (VHS) circular tubes under compression." *Thin Wall Struct. 2000*; 37: 223-240.

[9] Jiao, H., and Zhao, X. L. "Section slenderness limits of very high strength circular steel tubes in bending." *Thin Wall Struct*. 2004; 42(9): 1257-1271.

[10] Ma, J. L., Chan, T. M., and Young, B. "Experimental investigation of cold-formed high strength steel tubular beams." *Engineering Structures. 2015*; 126: 200-209.

[11] Ma, J. L., Chan, T. M., and Young, B. "Experimental investigation on stub column behavior of cold-formed high strength steel tubular sections." *J. Struct. Eng.2016;* 142(5): 04015174.

[12] Ma, J. L., Chan, T. M., and Young, B. "Material properties and residual stresses of cold-formed high strength steel hollow sections." *Journal of Constructional Steel Research*. 2015; 109: 152-165.

[13] Yu, C. K., and Tall, L. "Welded built-Up and Rolled Heat-Treated "T-1" Steel Columns - A514 Steel Beam-Columns." Lehigh University, Bethlehem, Pennsylvania; 1968.

[14] Usami, T., and Fukumoto, Y. "Local and Overall Buckling of Welded Box Columns." *ASCE*. 1982; 108.

[15] Zhang, L., Wang, F., Liang, Y., Zhao, O. (2019). Press-braked S690 high strength steel equal-leg angle and plain channel section stub columns: Testing, numerical simulation and design. Engineering Structures, 201, 109764.

[16] Wang, F., Liang, Y., Zhao, O. (2020). Experimental and numerical studies of pin-ended press-braked S960 ultra-high strength steel channel section columns. Engineering Structures, 215, 110629.

[17] Sun, Y., He, A., Liang, Y., Zhao, O. (2019). In-plane bending behaviour and capacities of S690 high strength steel welded I-section beams. Journal of Constructional Steel Research, 162, 105741.

[18] Sun, Y., Liang, Y., Zhao, O. (2019). Testing, numerical modelling and design of S690 high strength steel welded I-section stub columns. Journal of Constructional Steel Research, 159, 521–533.

[19] Ma, J. L., Chan, T. M., and Young, B. "Cold-Formed High-Strength Steel Rectangular and Square Hollow Sections under Combined Compression and Bending." Journal of Structural Engineering, ASCE; 2019; 145(12): 04019154

[20] Zhu, J.H., and Young, B. "Aluminum alloy circular hollow section beam-columns." *Thin-Walled Struct. 2006*; 44: 131-140.

[21] Huang, Y., and Young, B. "Design of cold-formed lean duplex stainless steel members in combined compression and bending." *J. Struct. Eng.*2014; 76:105-117.

[22] AS 4100. "Steel structures." Australian Standard, Sydney, Australia; 1998.

[23] ANSI/AISC 360-10 "Specification for structural steel buildings." American Institude of Steel Construction, Chicago, Illinois;2010.

[24] EN 1993-1-1 (2005). "Eurocode 3: Design of steel structures - Part 1-1: General rules and rules for buildings." CEN, Brussels, Belgium.

[25] EN 1993-1-6 (2005). "Eurocode 3: Design of steel structures - Part 1-6: Strength and Stability of Shell Structures." CEN, Brussels, Belgium.

[26] Chan, T. M., Zhao, X. L., and Young, B. "Cross-section classification for cold-formed and built-up high strength carbon and stainless steel tubes under compression." *Journal of Constructional Steel Research*. 2015;106: 289-295.

[27] ABAQUS. *ABAQUS Documentation*, Dassault Systèmes, Providence, RI, USA;2013.

[28] Rasmussen, K. J. R., and Hancock, G. J. "Design of cold-formed stainless steel tubular members. I:columns." *J. Struct. Eng*.1993; 119(8): 2349-2367.

[29] Gardner, L., and Nethercot, D. A. "Numerical modeling of stainless steel strucutral components - a consistent approach." *Journal of Structural Engineering*. 2004;130(10): 1586-1601.

[30] Yun, X., and Gardner, L. "The continuous strength method for the design of cold-formed steel non-slender tubular cross-sections." *Engineering Structures*. 2018; 549-564.

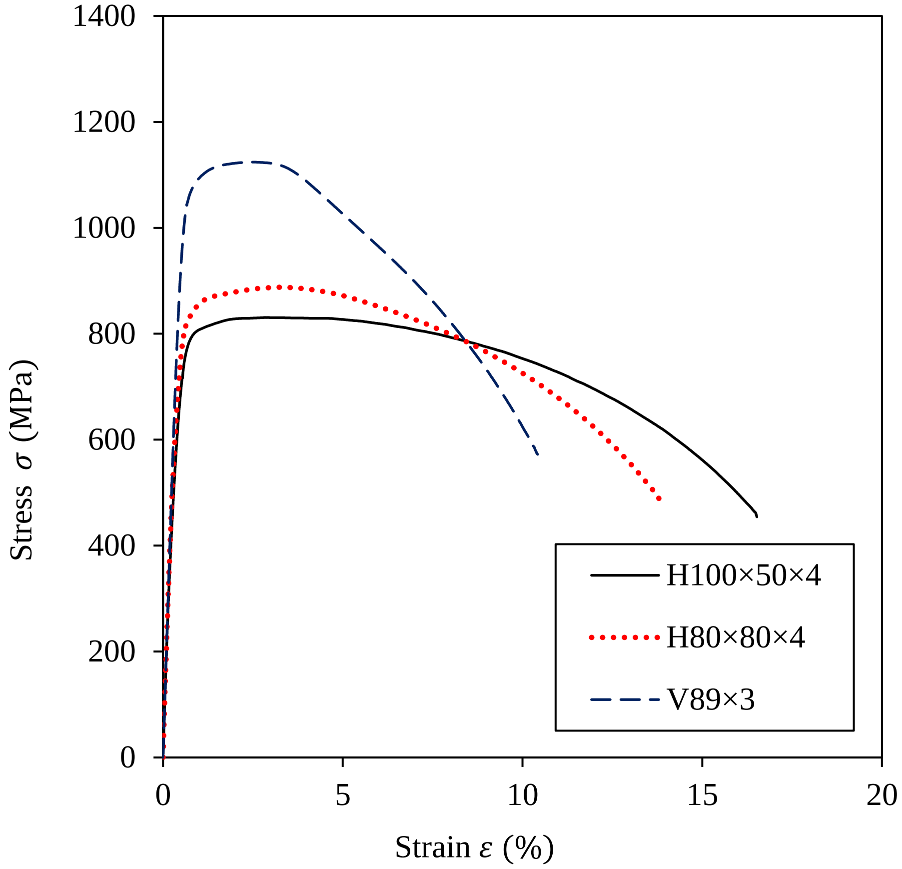

Fig. 1 . Obtained full stress-strain curves for three sections

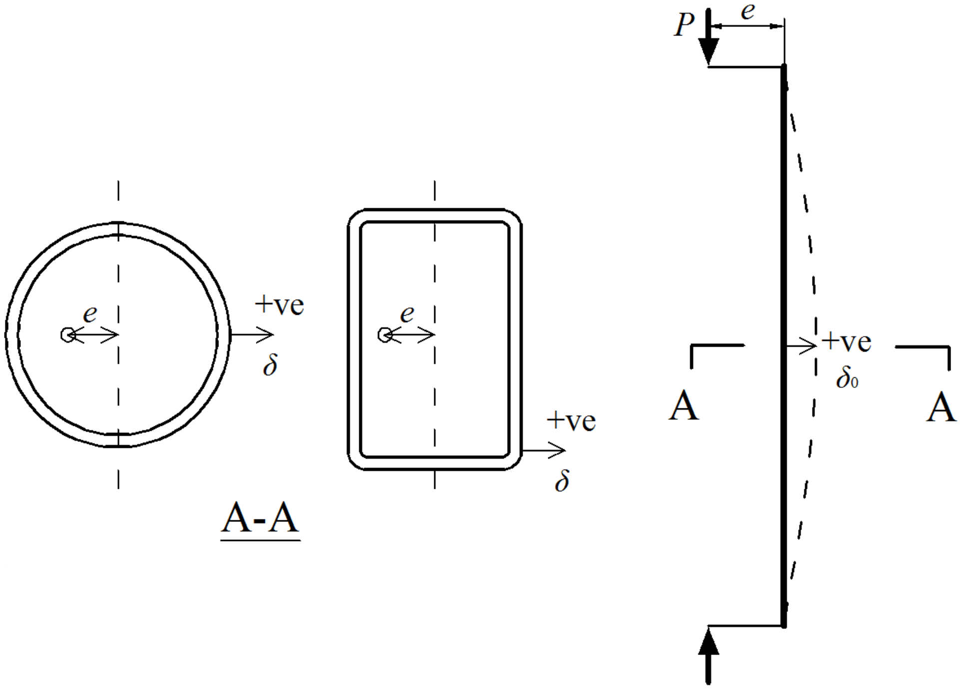

Fig. 2 . Sign convention and location of global geometric imiperfection measurements

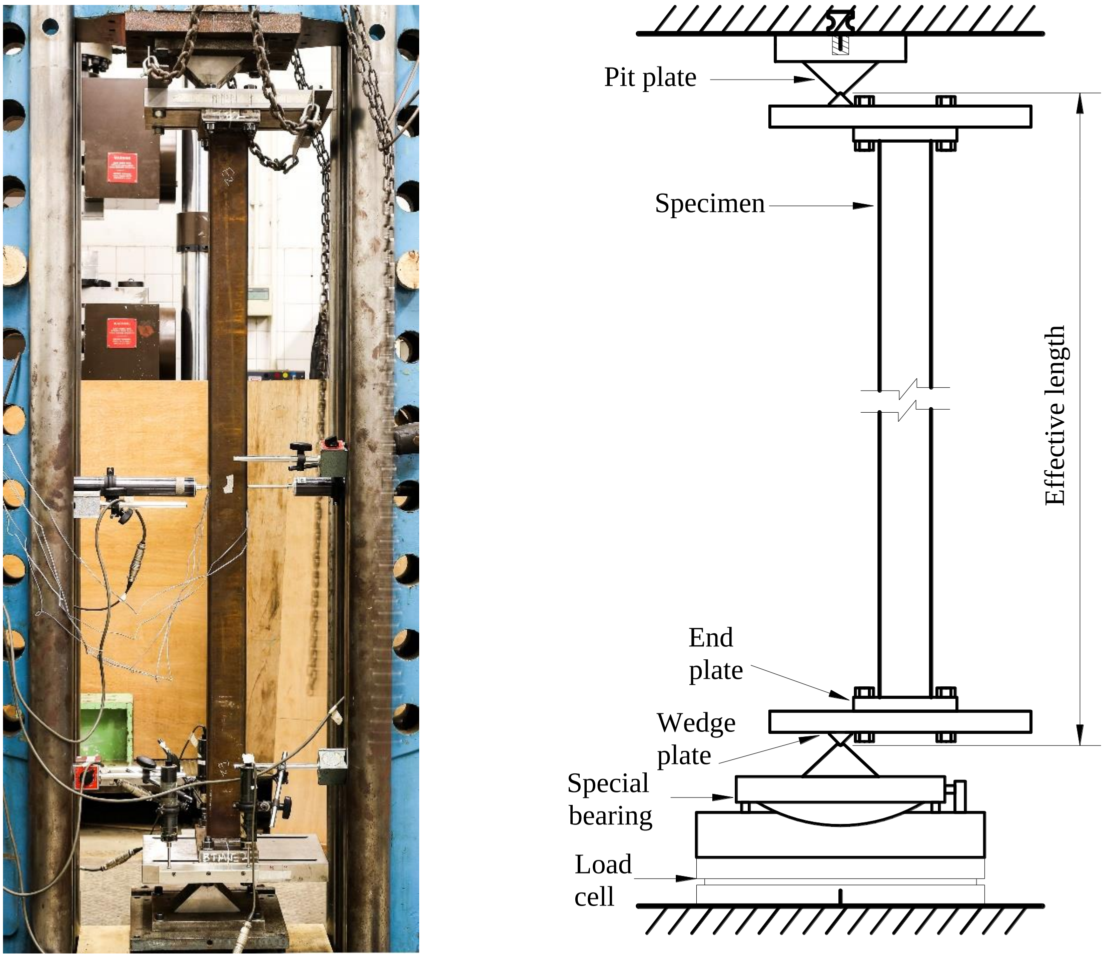

Fig. 3 . Experimental and schematic arrangement for beam-column tests

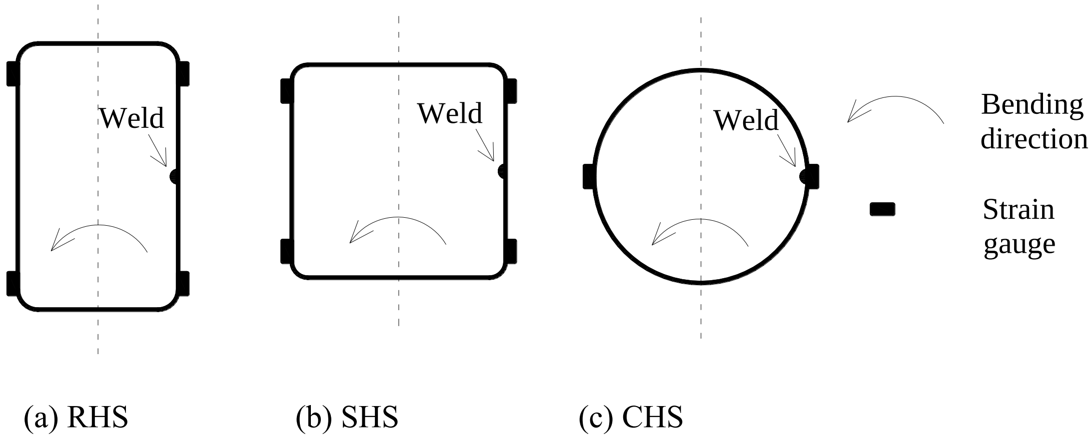

Fig. 4 . Arrangement of strain gauges for beam-columns

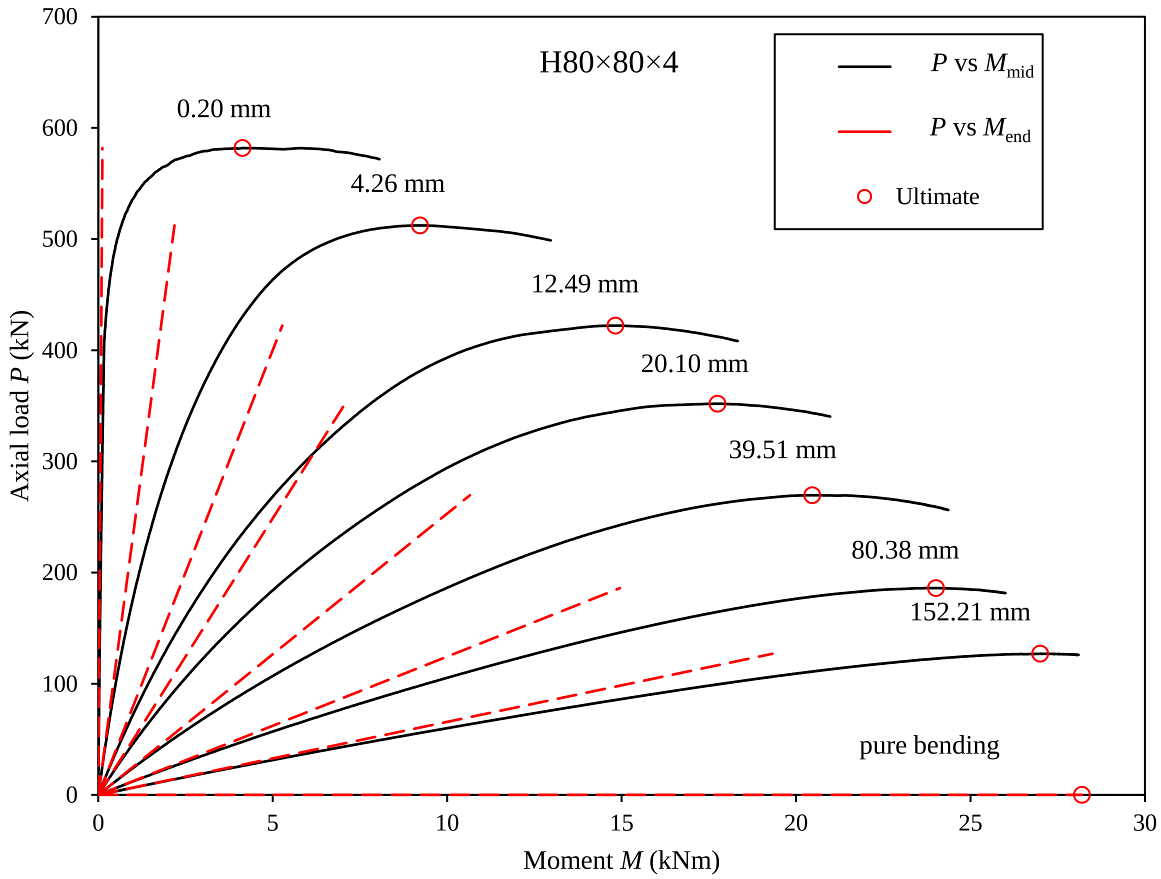

Fig. 5 . Axial load versus moment for series H80×80×4

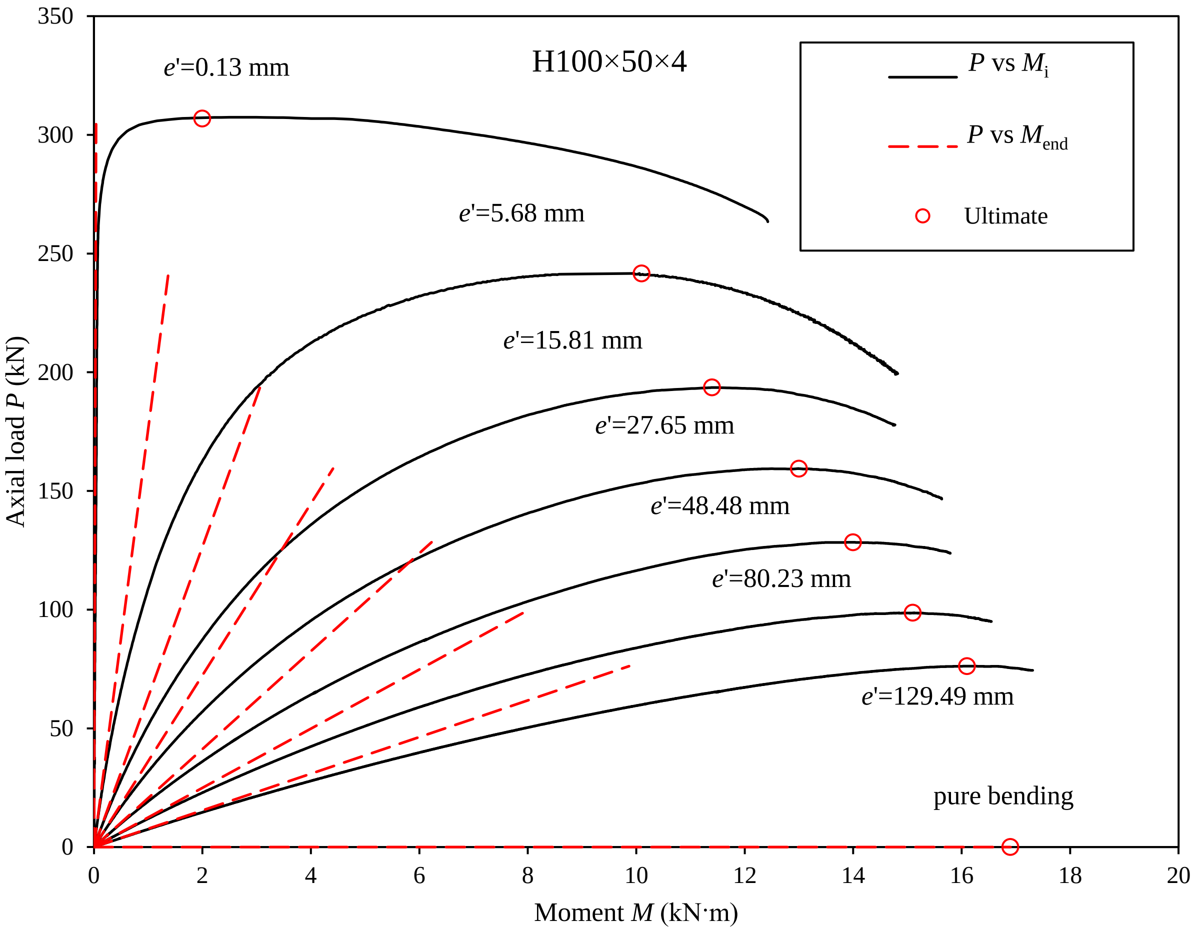

Fig. 6 . Axial load versus moment for series H100×50×4

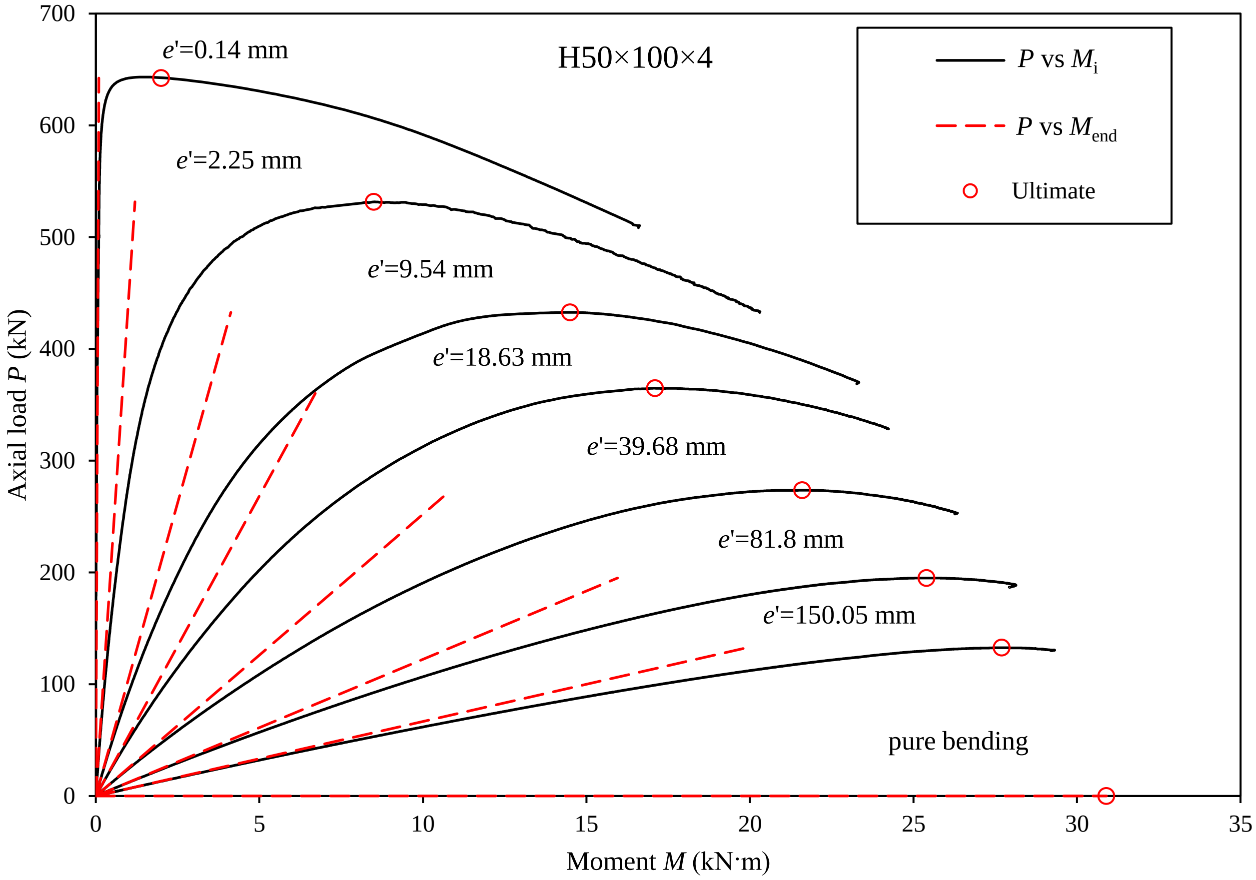

Fig. 7 . Axial load versus moment for series H50×100×4

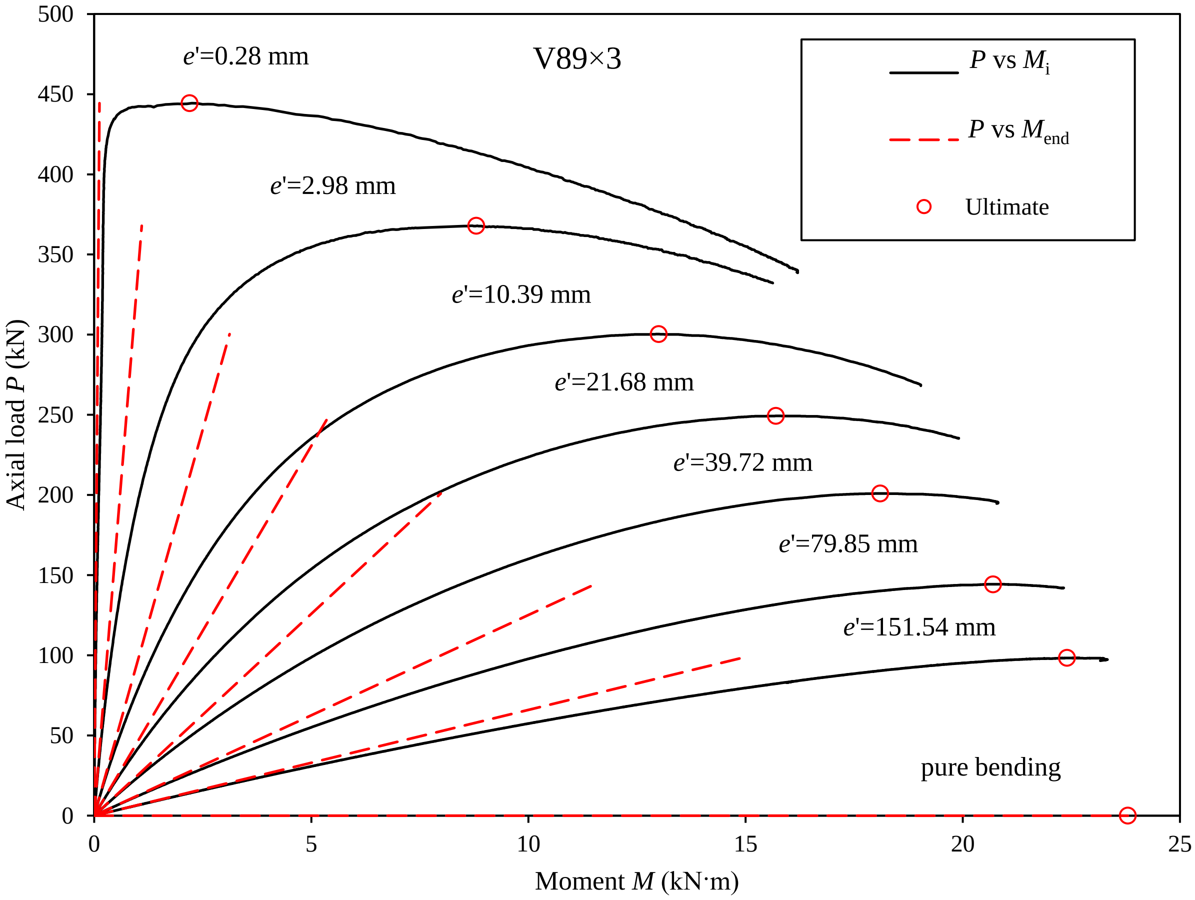

Fig. 8 . Axial load versus moment for series V89×3

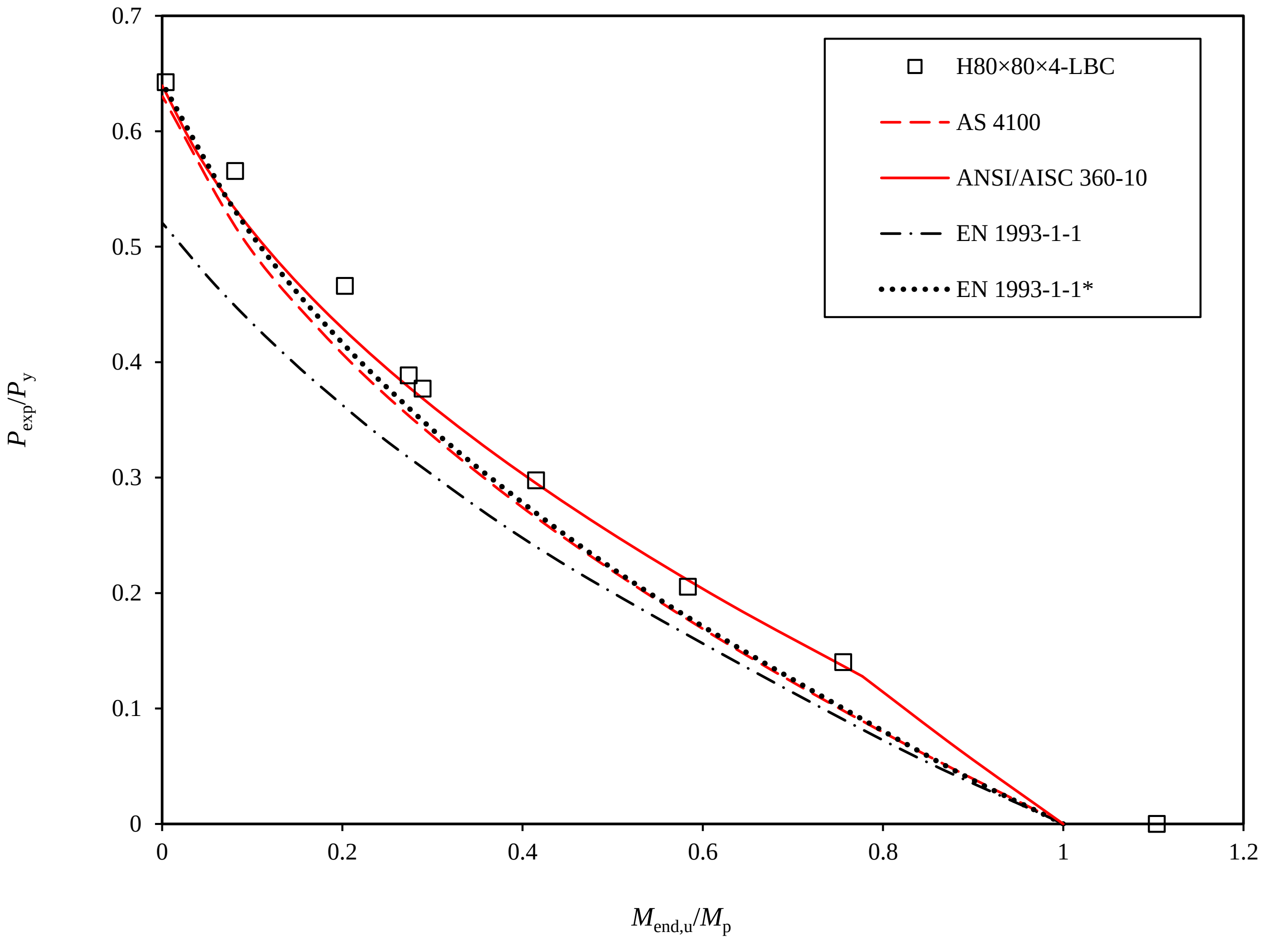

Fig. 9 . Comparison of interaction curves for H80×80×4

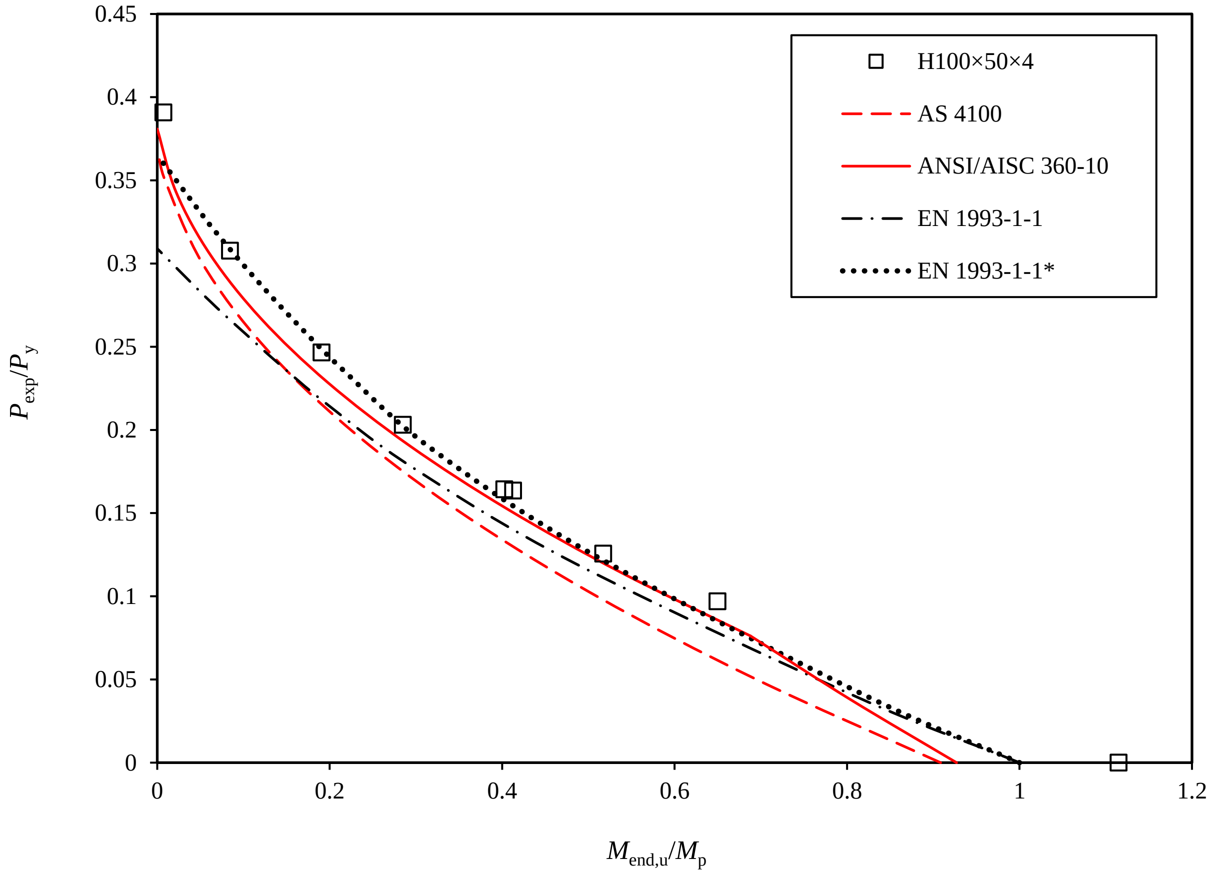

Fig. 10 . Comparison of interaction curves for H100×50×4

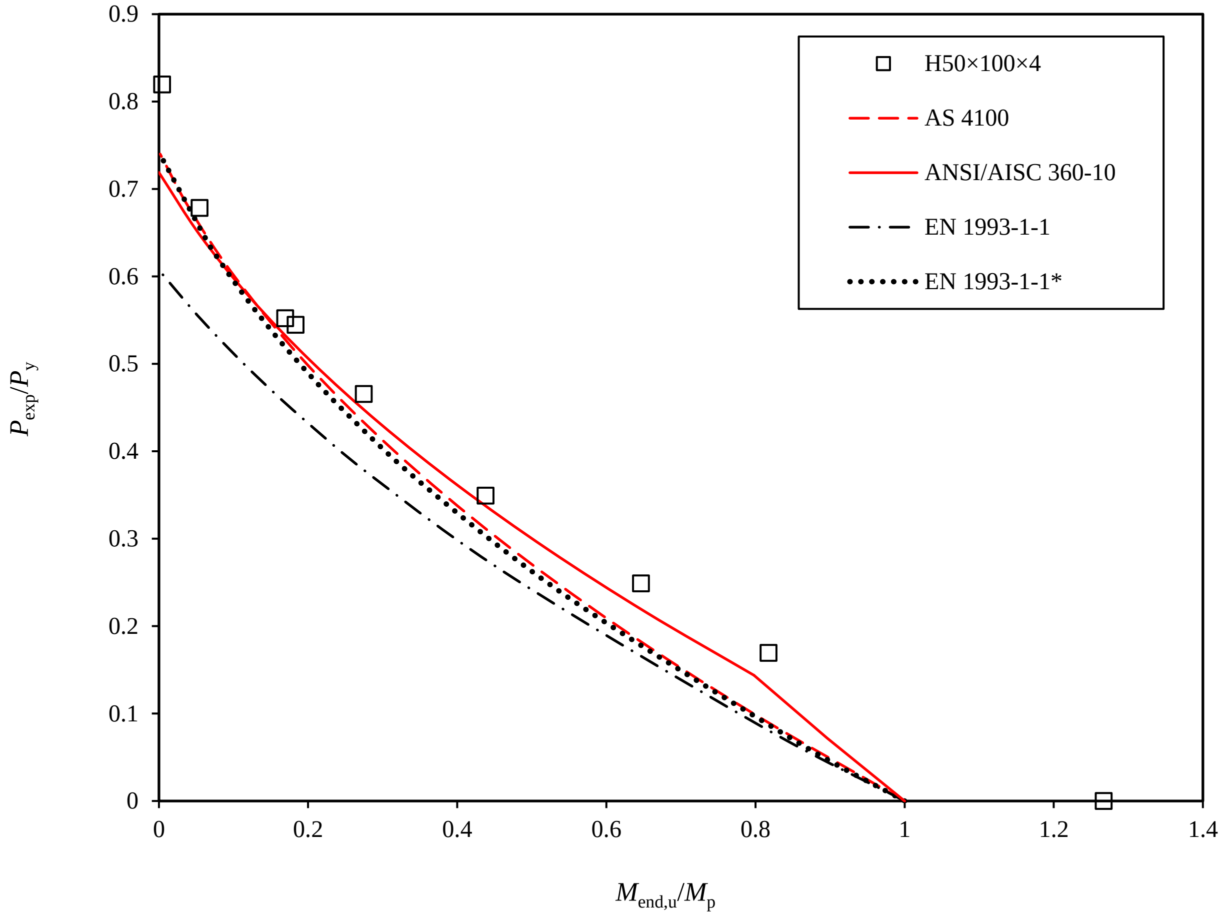

Fig. 11 . Comparison of interaction curves for H50×100×4

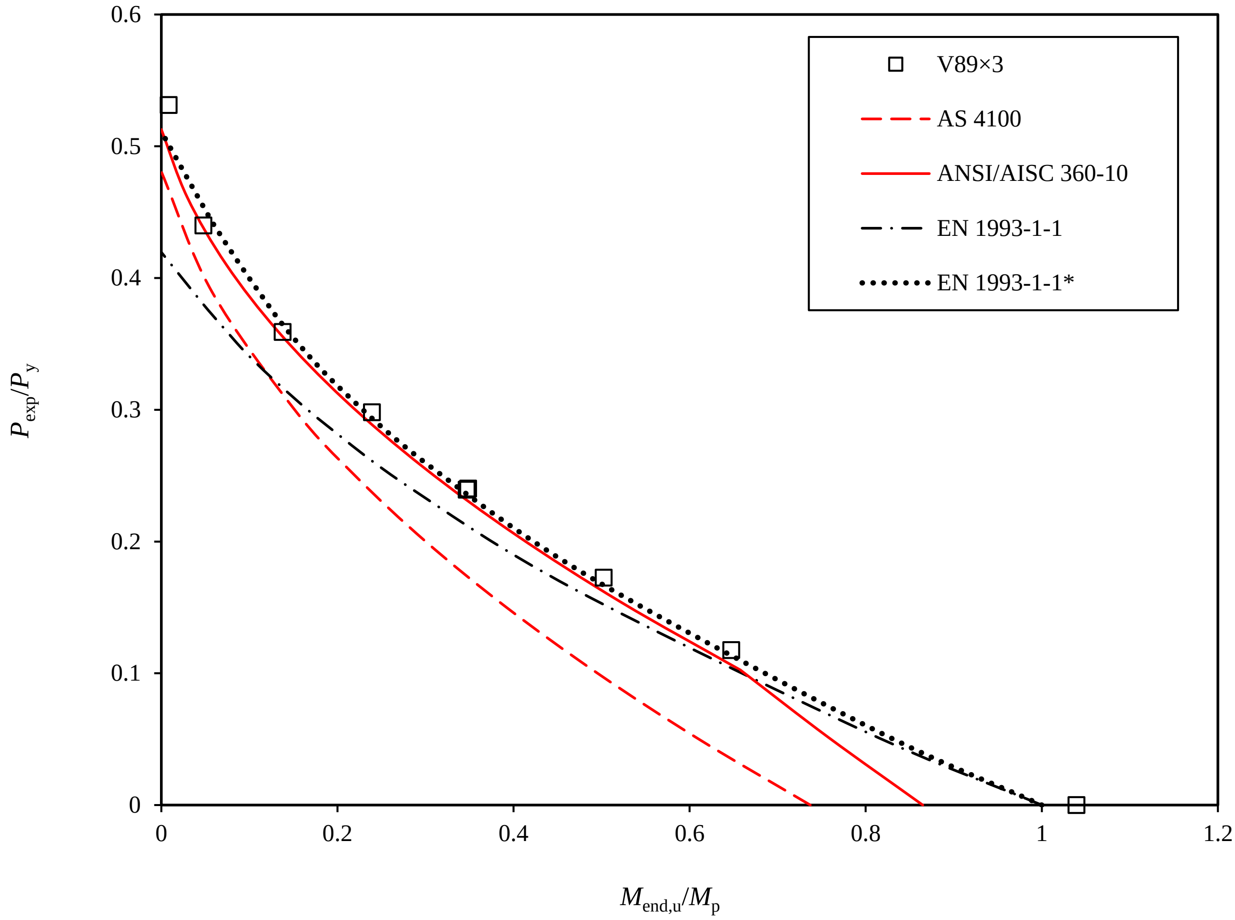

Fig. 12 . Comparison of interaction curves for V89×3

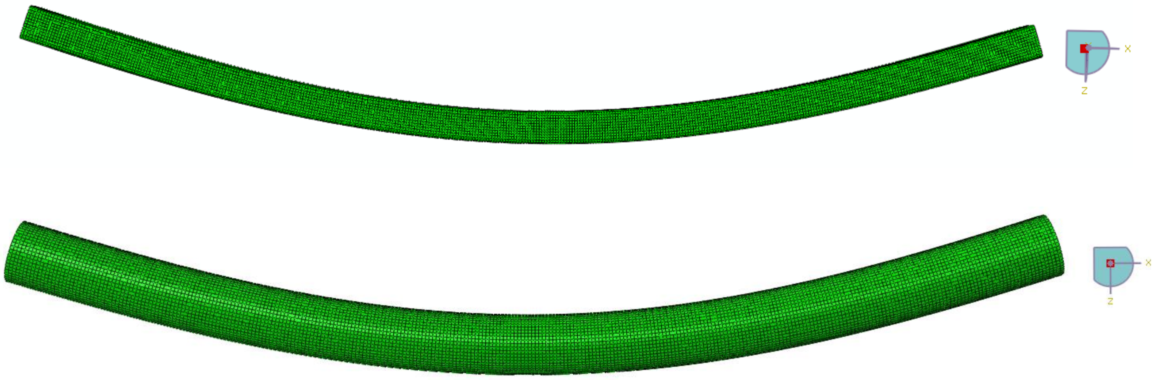

Fig. 13 . Global imperfection profile for H100×50×4 and V89×3

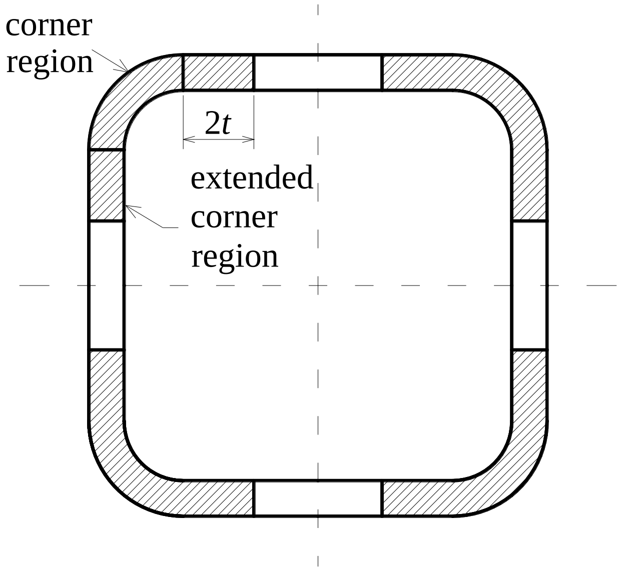

Fig. 14 . Extension of corner material property to flat portions

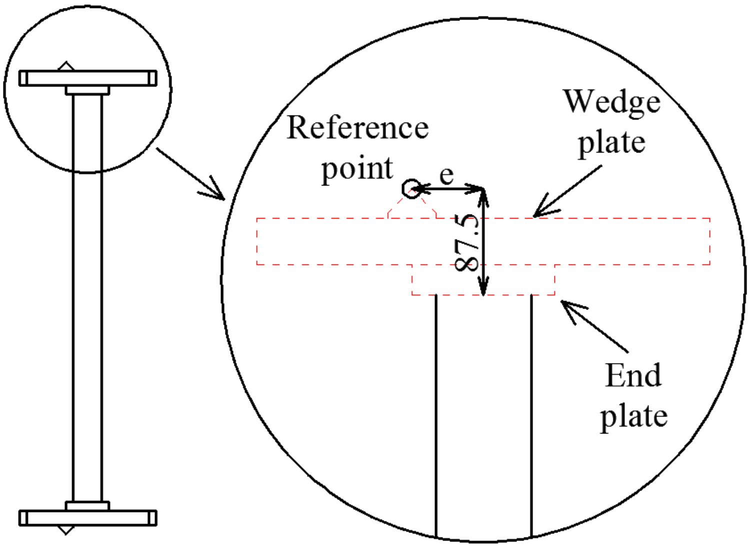

Fig. 15 . Location of reference point

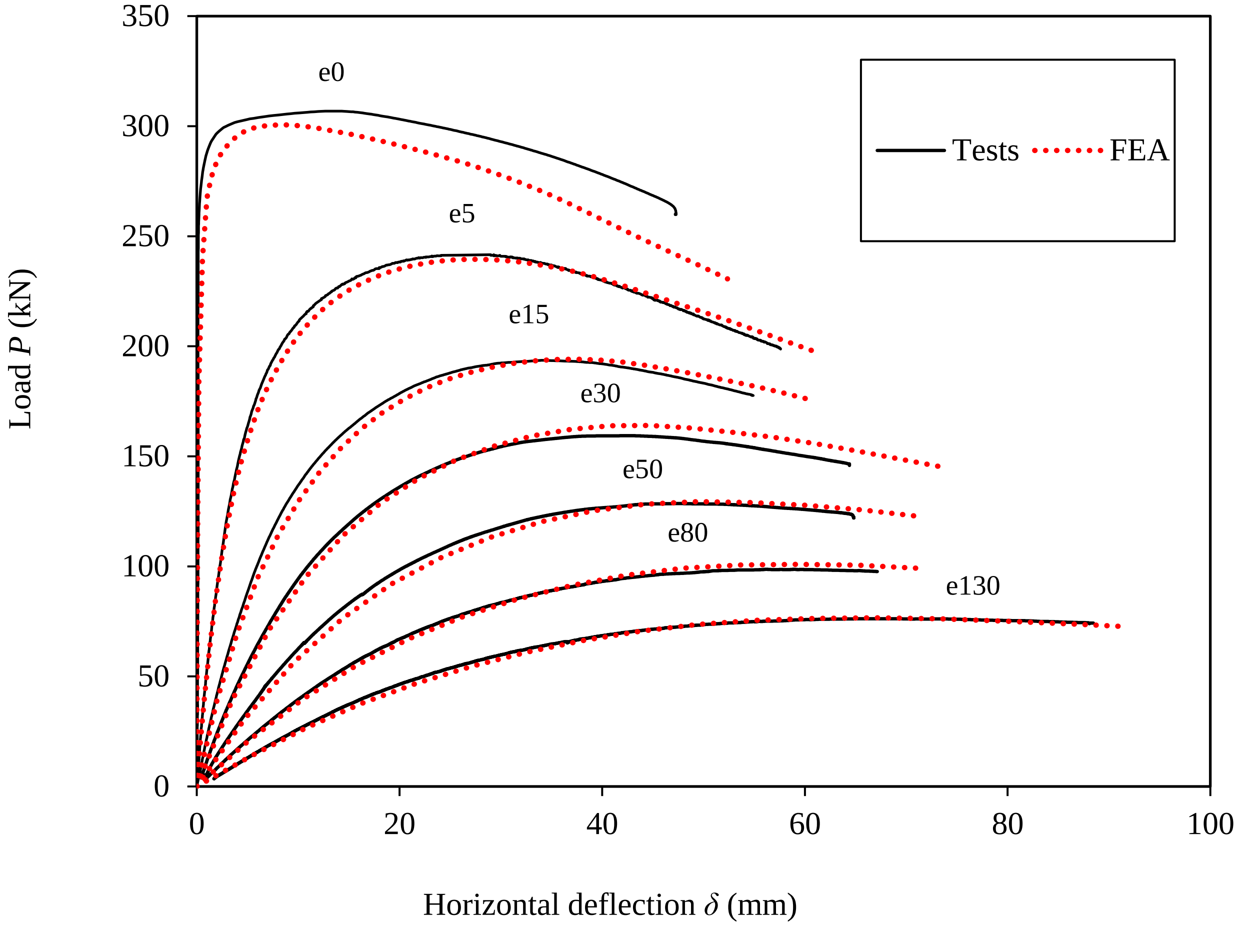

Fig. 16 . Experimental and numercial load-delfection curves for H100×50×4

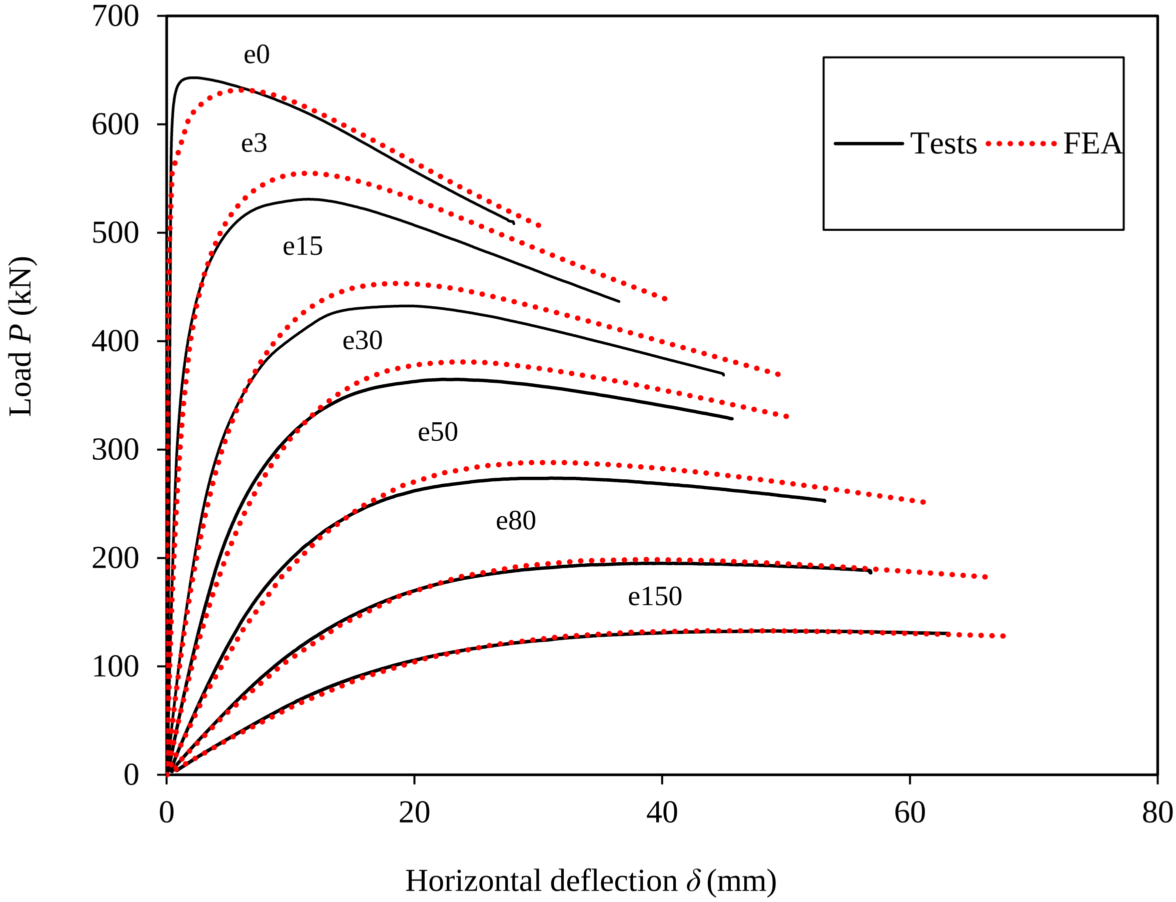

Fig. 17 . Experimental and numercial load-delfection curves for H50×100×4

Fig. 18 . Comparison of failure modes between test and numerical results for H50×100×4-BC-e0, H100×50×4-BC-e5, H80×80×4-BC-e40, V89×3-BC-e150 (from left to right)

Table 1. Tensile coupon test results

Section	E (GPa)	$\sigma_{0.2}$ (MPa)	σ_u (MPa)	ε_{25mm} (%)
H80×80×4	218	792	888	14
H100×50×4	208	724	831	17
V89×3	209	1054	1124	10

Table 2. Specimen dimensions and measured eccentricities of series H80×80×4

Specimen	B (mm)	D (mm)	t (mm)	R (mm)	r (mm)	A (mm^2)	W_{el} (×10^3 mm^3)	W_{pl} (×10^3 mm^3)	$e+\delta_0$ (mm)
H80×80×4-BC-e0	80.3	80.1	3.94	9.5	5.0	1145	27.0	32.2	0.20
H80×80×4-BC-e5	80.2	80.1	3.93	9.5	5.0	1142	26.9	32.1	4.26
H80×80×4-BC-e10	80.3	80.1	3.91	9.5	5.0	1138	26.8	32.0	12.49
H80×80×4-BC-e20	80.3	80.2	3.91	9.5	5.0	1137	26.8	32.0	20.10
H80×80×4-BC-e20#	80.4	80.2	3.95	9.5	5.0	1151	27.1	32.4	22.13
H80×80×4-BC-e40	80.2	80.1	3.93	9.5	5.0	1143	26.9	32.1	39.51
H80×80×4-BC-e80	80.3	80.1	3.94	9.5	5.0	1146	27.0	32.2	80.38
H80×80×4-BC-e150	80.4	80.2	3.94	9.5	5.0	1147	27.0	32.2	152.21

Table 3. Specimen dimensions and measured eccentricities of series H100×50×4

Specimen	B (mm)	D (mm)	t (mm)	R (mm)	r (mm)	A (mm^2)	W_{el} (×10^3 mm^3)	W_{pl} (×10^3 mm^3)	$e+\delta_0$ (mm)
H100×50×4-BC-e0	100.2	50.6	3.97	8.5	3.5	1082	18.0	20.9	0.13
H100×50×4-BC-e5	100.3	50.5	3.98	8.5	3.5	1085	18.0	20.9	5.68
H100×50×4-BC-e15	100.2	50.6	3.96	8.5	3.5	1080	18.0	20.9	15.81
H100×50×4-BC-e30	100.3	50.6	4.00	8.5	3.5	1091	18.1	21.1	27.65
H100×50×4-BC-e50	100.3	50.6	3.97	8.5	3.5	1082	18.0	20.9	48.48
H100×50×4-BC-e50#	100.2	50.5	3.97	8.5	3.5	1083	17.9	20.9	47.18
H100×50×4-BC-e80	100.4	50.5	3.98	8.5	3.5	1086	18.0	20.9	80.23
H100×50×4-BC-e130	100.3	50.6	3.98	8.5	3.5	1085	18.0	21.0	129.49

Table 4. Specimen dimensions and measured eccentricities of series H50×100×4

Specimen	B (mm)	D (mm)	t (mm)	R (mm)	r (mm)	A (mm^2)	W_{el} (×10^3 mm^3)	W_{pl} (×10^3 mm^3)	$e+\delta_0$ (mm)
H50×100×4-BC-e0	50.3	100.2	3.98	8.5	3.5	1083	26.5	33.7	0.14
H50×100×4-BC-e3	50.5	100.2	3.97	8.5	3.5	1081	26.4	33.6	2.25
H50×100×4-BC-e10	50.6	100.1	3.98	8.5	3.5	1086	26.6	33.8	9.54
H50×100×4-BC-e10#	50.5	100.3	3.95	8.5	3.5	1078	26.4	33.6	9.96
H50×100×4-BC-e20	50.6	100.2	3.96	8.5	3.5	1080	26.4	33.6	18.63
H50×100×4-BC-e40	50.6	100.1	3.97	8.5	3.5	1082	26.5	33.7	39.68
H50×100×4-BC-e80	50.5	100.2	3.98	8.5	3.5	1084	26.5	33.8	81.80
H50×100×4-BC-e150	50.4	100.2	3.98	8.5	3.5	1085	26.5	33.7	150.05

Table 5. Specimen dimensions and measured eccentricities of series V89×3

Specimen	D (mm)	t (mm)	A (mm^2)	W_{el} ($\times 10^3$ mm^3)	W_{pl} ($\times 10^3$ mm^3)	$e + \delta_0$ (mm)
V89×3-BC-e0	89.0	2.93	792	16.5	21.7	0.28
V89×3-BC-e3	88.9	2.94	794	16.5	21.8	2.98
V89×3-BC-e10	88.9	2.92	790	16.4	21.6	10.39
V89×3-BC-e20	88.9	2.94	795	16.5	21.7	21.68
V89×3-BC-e40	89.0	2.95	798	16.6	21.9	39.72
V89×3-BC-e40#	88.9	2.93	790	16.4	21.6	39.61
V89×3-BC-e80	89.0	2.94	794	16.5	21.8	79.85
V89×3-BC-e150	88.8	2.94	793	16.5	21.7	151.54

Table 6. Measured global geometric imperfections at mid-length

Specimen	δ_0 (mm)	δ_0/L
H80×80×4-BC-e0	0.381	1/3885
H80×80×4-BC-e5	0.229	1/6474
H80×80×4-BC-e10	0.254	1/5827
H80×80×4-BC-e20	0.292	1/5067
H80×80×4-BC-e20#	0.571	1/2590
H80×80×4-BC-e40	0.317	1/4661
H80×80×4-BC-e80	0.508	1/2913
H80×80×4-BC-e150	0.635	1/2331
H100×50×4-BC-e0	-0.229	-1/6474
H100×50×4-BC-e5	0.381	1/3885
H100×50×4-BC-e15	0.889	1/1665
H100×50×4-BC-e30	0.571	1/2590
H100×50×4-BC-e50	-0.254	-1/5827
H100×50×4-BC-e50#	-0.127	-1/11654
H100×50×4-BC-e80	0.762	1/1942
H100×50×4-BC-e130	0.191	1/7769
H50×100×4-BC-e0	-0.025	-1/58268
H50×100×4-BC-e3	-0.254	-1/5827
H50×100×4-BC-e10	0.000	0
H50×100×4-BC-e10#	-0.508	-1/2913
H50×100×4-BC-e20	0.254	1/5827
H50×100×4-BC-e40	0.635	1/2331
H50×100×4-BC-e80	0.953	1/1554
H50×100×4--BC-e150	-0.254	-1/5827
V89×3-BC-e0	-0.152	-1/9711
V89×3-BC-e3	0.000	0
V89×3-BC-e10	-0.114	-1/12948
V89×3-BC-e20	-0.292	-1/5067
V89×3-BC-e40	0.000	0
V89×3-BC-e40#	-0.063	-1/23307
V89×3-BC-e80	0.152	1/9711
V89×3-BC-e150	0.889	1/1665

Repeated test

Table 7. Measured bending moment capacities

Specimen	Ultimate moment capacity M_{exp} (kNm)
H80×80×4-B	28.1
H100×50×4-B	16.9
H50×100×4-B	30.9
V89×3-B	23.8

Table 8. Beam-column test results

Specimen	P_{exp} (kN)	$M_{end,u}$ (kNm)	$M_{mid,u}$ (kNm)	θ (Rad)	P_{exp}/P_{AS}	P_{exp}/P_{AISC}	P_{exp}/P_{EC3}	P_{exp}/P_{EC3}^{*}
H100×50×4-BC-e0	306.9	0.1	2.0	0.013	1.06	1.03	1.27	1.07
H100×50×4-BC-e5	241.6	1.3	10.1	0.061	1.10	1.06	1.14	1.00
H100×50×4-BC-e15	193.6	2.9	11.4	0.080	1.10	1.05	1.09	0.99
H100×50×4-BC-e30	159.4	4.3	13.0	0.091	1.09	1.02	1.07	0.99
H100×50×4-BC-e50	128.4	6.3	14.0	0.111	1.13	1.05	1.09	1.03
H100×50×4-BC-e50#	129.0	6.1	14.0	0.114	1.12	1.04	1.08	1.02
H100×50×4-BC-e80	98.7	7.8	15.1	0.136	1.11	1.02	1.06	1.02
H100×50×4-BC-e130	76.2	9.8	16.1	0.149	1.15	1.04	1.08	1.05
H50×100×4-BC-e0	642.3	0.1	2.0	0.007	1.10	1.14	1.35	1.10
H50×100×4-BC-e3	531.6	1.3	8.5	0.027	1.03	1.04	1.21	1.03
H50×100×4-BC-e10	432.7	4.1	14.5	0.041	1.03	1.03	1.16	1.03
H50×100×4-BC-e10#	426.9	4.5	14.6	0.043	1.05	1.04	1.17	1.05
H50×100×4-BC-e20	364.8	6.7	17.1	0.053	1.05	1.03	1.15	1.06
H50×100×4-BC-e40	273.6	10.7	21.6	0.072	1.06	1.02	1.14	1.07
H50×100×4-BC-e80	195.0	15.8	25.4	0.089	1.12	1.05	1.17	1.12
H50×100×4-BC-e150	132.7	19.9	27.7	0.115	1.15	1.06	1.19	1.15
H80×80×4-BC-e0	581.9	0.1	4.1	0.016	1.02	1.00	1.23	1.00
H80×80×4-BC-e5	512.3	2.1	9.2	0.027	1.08	1.06	1.23	1.06
H80×80×4-BC-e10	422.2	5.2	14.8	0.044	1.11	1.07	1.22	1.09
H80×80×4-BC-e20	351.9	7.0	17.8	0.057	1.07	1.02	1.15	1.06
H80×80×4-BC-e20#	341.5	7.4	18.3	0.060	1.06	1.01	1.14	1.04
H80×80×4-BC-e40	269.6	10.6	20.5	0.071	1.06	1.01	1.13	1.06
H80×80×4-BC-e80	186.0	14.9	24.0	0.092	1.06	0.99	1.10	1.06
H80×80×4-BC-e150	127.0	19.2	27.0	0.123	1.09	1.01	1.12	1.09
V89×3-BC-e0	444.4	0.2	2.2	0.010	1.11	1.04	1.27	1.04
V89×3-BC-e3	367.9	1.1	8.8	0.039	1.08	1.00	1.14	0.97
V89×3-BC-e10	300.3	3.2	13.0	0.062	1.12	1.01	1.11	0.99
V89×3-BC-e20	249.3	5.5	15.7	0.076	1.15	1.02	1.10	1.01
V89×3-BC-e40	200.9	8.0	18.1	0.092	1.17	1.02	1.07	1.01
V89×3-BC-e40#	200.1	7.9	18.2	0.098	1.18	1.02	1.08	1.01
V89×3-BC-e80	144.3	11.5	20.7	0.123	1.22	1.03	1.06	1.01
V89×3-BC-e150	98.4	14.8	22.4	0.149	1.27	1.04	1.05	1.02
			mean		1.10	1.03	1.14	1.04
			COV		0.051	0.027	0.062	0.039

Repeated test

Table 9. Design interaction equations

Design standards	Interaction equation
ANSI/AISC 360-10	$\begin{cases} \frac{P_u}{P_n}+\frac{8}{9}\frac{M_u}{M_n}\leq 1 & for\ \frac{P_u}{P_n}\geq 0.2 \\ \frac{P_u}{2P_n}+\frac{M_u}{M_n}\leq 1 & for\ \frac{P_u}{P_n}< 0.2 \end{cases}$ $M_u=\frac{M_{end,u}}{(1-P/P_{cr})}$
AS4100	$\frac{P_u}{P_n}+\frac{M_u}{M_n}\leq 1$
EN1993	$\frac{P_u}{P_n}+k_{yy}\frac{M_{end,u}}{M_n}\leq 1$

Table 10. Comparison of beam-column test results with FE results

Specimen	P_{exp} / P_{FEA}
H50×100×4-BC-e0	1.02
H50×100×4-BC-e3	0.96
H50×100×4-BC-e10	0.95
H50×100×4-BC-e10#	0.96
H50×100×4-BC-e20	0.96
H50×100×4-BC-e40	0.95
H50×100×4-BC-e80	0.98
H50×100×4-BC-e150	1.00
H100×50×4-BC-e0	1.02
H100×50×4-BC-e5	1.01
H100×50×4-BC-e15	1.00
H100×50×4-BC-e30	0.97
H100×50×4-BC-e50	0.99
H100×50×4-BC-e50#	0.99
H100×50×4-BC-e80	0.98
H100×50×4-BC-e130	0.99
H80×80×4-BC-e0	0.93
H80×80×4-BC-e3	0.99
H80×80×4-BC-e10	1.01
H80×80×4-BC-e20	0.97
H80×80×4-BC-e20#	0.96
H80×80×4-BC-e40	0.96
H80×80×4-BC-e80	0.95
H80×80×4-BC-e150	0.98
V89×3-BC-e0	0.91
V89×3-BC-e3	0.88

V89×3-BC-e10		0.91
V89×3-BC-e20		0.92
V89×3-BC-e40		0.93
V89×3-BC-e40#		0.94
V89×3-BC-e80		0.96
V89×3-BC-e150		0.98
	mean	0.97
	COV	0.035

Repeated test